Regular Article

Impact of a hybrid coating REBCO-CC-Cu to the resistive wall beam impedance of the FCC-hh beam screen

Nikki Tagdulang[1,2,a] , **Thomas Günzel**[1,b], **Patrick Krkotić**[3,c], **Sergio Calatroni**[3,d], **Juan Manuel O'Callaghan**[2,e], **Montse Pont**[1,f]

[1] ALBA Synchrotron, Carrer de la Llum, 2, 26, 08290 Cerdanyola del Valles, Spain
[2] Signal Theory and Communications, Universitat Politécnica de Catalunya, Carrer de Jordi Girona, 1-3, 08034 Barcelona, Spain
[3] Technology Department, CERN, Espl. des Particules 1, 1211 Meyrin, Switzerland

Abstract The Future Circular Hadron Collider design studies proposed a novel dual chamber beam screen consisting of copper and stainless steel. However, one concern about the current design is the inherent resistive wall beam impedance of the beam screen, which may not be low enough to guarantee stable beam operation especially critical on the vertical plane. In order to reduce the resistive wall beam impedance as much as possible while keeping the dipole field quality within specifications, a hybrid beam screen consisting of REBCO-CC and Cu is proposed for the inner chamber of the beam screen. We performed a comprehensive position and REBCO-CC content study, leading to an optimum configuration for a REBCO-CC-Cu hybrid design. These studies utilized measured values of REBCO-CC surface impedance obtained under realistic FCC-hh conditions. The calculations were carried out by combining numerical simulations and beam coupling impedance theory for general beam pipe cross sections, where we found a substantial decrease in the vertical resistive wall beam impedance by about an order of magnitude compared to the nominal beam screen design made of copper. Limitations of the proposed design and possible mitigation actions are also discussed.

1 Introduction

The Future Circular Hadron Collider (FCC-hh) [1] project aims to achieve a center of mass collision energy of around 100 TeV in the search for new physics beyond the standard model. Such unprecedented energy requires the use of superconducting Nb_3Sn dipole magnets that will generate a magnetic field of 16 T in a 100 km circumference ring. At the expected injection energy level of 3.3 TeV, these dipole magnets will produce an approximate magnetic field strength of 1 T.

The synchrotron power emitted by the circulating proton beam at the collision energy will have a linear power density of approximately 35 W/m. To protect the cold bore of the dipole magnets against this extremely high power compared to the Large Hadron Collider (LHC), a beam screen (BS) will be employed. The conductivity of the material of which the beam screen is made will have a significant impact on the resistive wall impedance; this will be a common problem for any future high-energy colliders [2], since all of them are projected to have large circumferences and large magnetic fields.

As shown in Fig. 1a, the nominal baseline design of the FCC-hh beam screen (as presented in the FCC Conceptual Design Report [1]) comprises two chambers: the inner chamber and the outer chamber. In addition, features designed to effectively absorb the intense synchrotron radiation and maintain the required vacuum conditions [3] are incorporated.

The inner chamber takes on a C-shaped configuration stacked vertically and symmetrically, featuring two slots. One of the two slots will allow the synchrotron radiation to pass through and be absorbed in the outer chamber, where the Cu has a sawtooth finishing for maximum photon absorption [3]. The opposite slot is there to ensure the mechanical stability of the assembly and ease of manufacturability. The inner chamber consists of a 1.00 mm thick P506 stainless steel (SS) sheet and 300 μm thick co-laminated oxygen-free electronic (OFE) Cu with a residual resistivity ratio of $RRR = 100$. The co-laminated Cu will be treated with Laser Ablation Surface Engineering (LASE) or coated with amorphous carbon (aC) to mitigate the build-up of e-cloud by lowering the secondary electron yield while keeping a low surface impedance [4]. The outer chamber, on the other hand, is composed of two
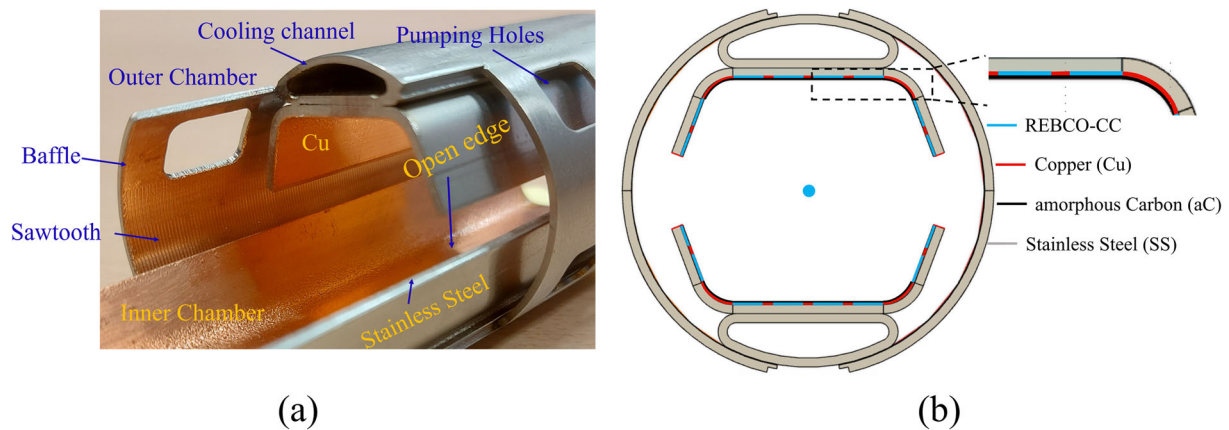
Fig. 1 a Nominal FCC-hh beam screen design consisting of Cu (orange), stainless steel (gray). **b** Example of an FCC-hh hybrid beam screen made of REBCO-CC (cyan), Cu (red), and covered with a thin layer of amorphous carbon (black). Figure adapted from [3]

lateral baffles constructed with a 1.00 mm thick P506 stainless steel (SS) sheet and 75 μm co-laminated Cu. Attached to it are the cooling channels to keep the temperature of the beam screen within 40-60 K for thermal efficiency. Along the outer chamber one can find a series of holes for effective pumping.

Previous studies [5] have shown that resistive wall beam impedance due to the finite conductivity of the BS is the primary source of impedance-induced instabilities. This is particularly critical in the vertical plane owing to the lower vertical aperture (24.44 mm) compared to the horizontal (27.65 mm) aperture of the inner chamber, as well as to the different aspect ratio due to the presence of the slots. While the current design of Fig. 1(a) has demonstrated [5] to exhibit sufficiently low resistive wall beam impedance, it is, however, close to the margin for safe operation.

To address this potential problem, high-temperature superconductors (HTS) in the form of REBa$_2$Cu$_3$O$_{7-x}$ coated conductor (REBCO-CC being RE = Y, Gd, Eu) have been proposed as an alternative to the co-laminated Cu of the inner chamber [6]. REBCO-CC technology is already available in kilometers length from several providers and, therefore, sufficiently mature for large-scale productions. With such a coating, one has to consider that the magnetic field generated by the persistent currents in the surface of the REBCO-CC will affect the magnetic field quality seen by the beam. Studies [7, 8] have shown that subdividing REBCO-CC into narrow parallel decoupled segments effectively reduces the magnetic field produced by the persistent currents and reduces the changes in the magnetic field uniformity. Consequently, the application of REBCO-CC as coatings for the FCC-hh will involve forming a hybrid ensemble of alternating strips of REBCO-CC and Cu. Figure 1(b) illustrates a possible example of a hybrid REBCO-CC-Cu beam screen.

Measurements of the secondary electron yield on REBCO-CC have indicated values close to 3 [6, 9], which are too high to ensure an operation free of e-cloud. To lower the yield, similar to the nominal beam screen, a layer of aC will have to be deposited on top of the HTS [6].

In this paper, we perform a comprehensive investigation of a hybrid beam screen consisting of alternate stripes of REBCO-CC and Cu building upon studies conducted [10–12]. We demonstrate, for the first time, the impact of REBCO-CC on the nominal design of the FCC-hh beam screen at the collision and injection energies using measured values of the surface impedance of REBCO-CC under challenging conditions, an external magnetic field of 16 T, at 50 K, and as a function of frequency, *i.e.,* as close as possible to the FCC-hh working conditions, and samples prepared mimicking a possible extensive production process.

This paper is organized as follows. In Sect. 2, we formulate a numerical procedure for the computation of resistive wall beam impedance in the FCC-hh. In Sect. 3, we introduce the surface impedance of REBCO-CC, copper, and stainless steel used in this study. In Sect. 4, we present a systematic study of the effect of REBCO-CC depending on its position on the beam screen and the percentage of coverage. The manufacturability of the hybrid beam screen is also studied, in view of resistive wall beam impedance. In Sect. 5, we demonstrate the impact of REBCO-CC at injection and collision energies of the FCC-hh, wherein we employ measured surface impedance values at 1 T and 16 T. The conclusions of the paper are given in Sect. 6.

2 Resistive wall beam impedance evaluation in the FCC-hh beam screen

Consider a proton beam with total charge Q circulating with a velocity equal to the speed of light ($v = c$) inside the beam pipe with drive current expressed in the frequency domain as

$$J_z = Q\delta(x - x_1)\delta(y - y_1)\exp(-jkz), \tag{1}$$

where x, y, and z refers to Cartesian coordinates in three dimensions. x_1, y_1, refer to the beam offsets along x and y coordinate with respect to the origin, and k is the wave number $k = \omega/c$, where ω is the angular frequency.

Generally, the longitudinal beam coupling impedance in the ultra-relativistic limit of a beam pipe with length L can be computed through [13]

$$Z_z(k) = -\frac{L}{|Q|^2} \oint E_z H_{1s}^* ds, \tag{2}$$

where the integral is taken over the beam pipe contour denoted by coordinate s. H_{1s}^* refers to the tangential component of the magnetic field $\mathbf{H}$ along a perfectly electrical conducting beam pipe wall; whereas, E_z is the longitudinal component of the electric field $\mathbf{E}$ for the case of a conducting beam pipe wall. The electromagnetic fields in Eq. (2) are computed at $x_1 = y_1 = 0$.

On the other hand, the transverse beam coupling impedance can be obtained assuming an axial dipole drive current of

$$J_z = Q\delta(x)[\delta(y - y_1) - \delta(y + y_1)]\exp(-jkz), \tag{3}$$

which leads to a vertical beam coupling impedance

$$Z_y(k) = -\frac{L}{|Q|^2}\frac{1}{4ky_1^2} \oint E_z H_{1s}^* ds, \tag{4}$$

when $y_1 \neq 0$. The horizontal beam coupling impedance can be calculated by replacing y with x in Eqs. (3) and (4).

The longitudinal component of the electric field, E_z, can be approximated using the Leontovich boundary condition or the surface impedance boundary condition (SIBC) [14, 15] through:

$$\mathbf{n} \times \mathbf{E} = Z_s \mathbf{n} \times \mathbf{n} \times \mathbf{H}, \tag{5}$$

valid for a smooth beam pipe wall with surface impedance Z_s, where $\mathbf{n}$ is the vector normal to the wall surface. Following Eq. (5),

$$E_z = -Z_s H_{1s}. \tag{6}$$

Substituting Eq. (6) into Eqs. (2) and (4) gives

$$Z_z(\omega) = \frac{L}{|Q|^2} \oint Z_s |H_{1s}|^2 ds \tag{7}$$

$$Z_y(\omega) = \frac{L}{|Q|^2}\frac{1}{4ky_1^2} \oint Z_s |H_{1s}|^2 ds. \tag{8}$$

Note that Z_s is a function of the tangential coordinate s, and being a material property it is also a function of frequency, ω, of magnetic field, B, and of temperature, T, while $|H_{1s}|$ is material independent and is only a function of s.

For simple geometrical structures, e.g., round, elliptical, and rectangular structures, there exist analytical solutions to the tangential magnetic field $|H_{1s}|$ [16, 17]. However for complex structures, the calculation of $|H_{1s}|$ can only be done numerically. To obtain $|H_{1s}|$ for the FCC-hh beam screen, we have used the commercially available 3D electromagnetic solver, Wakefield Solver of Particle Studio, available in Computer Simulation Technology (CST) [18].

CST's Wakefield Solver uses a finite integration technique to calculate the wake potential in the time domain and subsequently, the beam coupling impedance through Fast Fourier Transform (FFT). For smooth beam pipe structures of invariable geometry, the beam coupling impedance only consists of resistive wall beam impedance. The calculations of wakes are carried out from the source to a distance defined by the user which is called wake length. To ensure precise FFT implementation, it is crucial to select a wake length that is long enough to demonstrate vanishing wakes but not so long that it significantly increases computational time [19]. Thus, apart from the numerical noise level per length, the wake length is one of the defining parameters of the accuracy in the simulations, especially at low frequencies. Using the conventional approach of calculating resistive wall beam impedance, high inaccuracies can be found for highly conducting materials where the wakes tend to decay over very long distances. To circumvent this, we developed an approach combining CST and beam coupling impedance theory through Eqs. (7) and (8), although other computational approaches can also be used for the same purpose [15, 20–22]. This approach avoids the complete discretization of structures made up of thin material layers and repetitive discretization of the same structures with varying material compositions which require time-consuming computations. Another option of using CST was introduced by [19] employing a scaling technique. This method, however, leads to more computational effort since it requires separate simulations to account for beam coupling impedance at low frequencies.

The calculations using the aforementioned approach were carried out as follows. First, we calculated the tangential magnetic field $|H_{1s}|$ of a perfectly electrical conducting (PEC) pipe in CST. For the longitudinal beam coupling impedance calculation, the source and test beam were both situated at ($x = 0$, $y = 0$), e.g., at the center of the BS. For the vertical beam coupling impedance, the calculations were performed twice at opposing offsets, which corresponds to transverse offsets ($x = 0$, $y = y_1$) and ($x = 0$, $y = -y_1$). This allows computations with dipole drive current $J_z = J_z(y = y_1) - J_z(y = -y_1)$ [23, 24] giving $|H_{1s}| = ||H_{1s}(y = y_1)| - |H_{1s}(y = -y_1)||$. The horizontal beam coupling impedance was done in the same manner with offsets

Fig. 2 Close integration path for
the calculations of the resistive
wall beam impedance
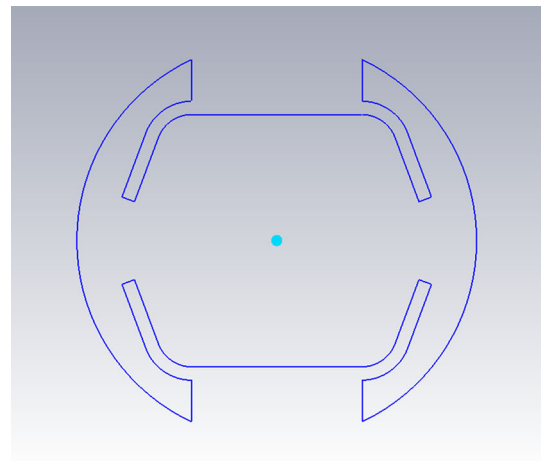
along the x plane. In this study, we used offsets of 1 mm, which are about 8% of the vertical aperture to minimize as much as possible nonlinear components without compromising accuracy from the need to mesh the setup sufficiently. Throughout our simulations, we utilized a wake length of 1000 mm for a beam screen length of 50 mm. Subsequently, we conducted the resistive wall beam impedance calculations in MATLAB [25]. The software structure follows by defining the tangential magnetic field and surface impedance at the boundary. Thereafter, we performed numerical integration utilizing Eqs. (7) and (8) using the trapezoidal integration function available in MATLAB.

In our calculations of the resistive wall beam impedance for the FCC-hh, analogous to [26] we have adopted the following simplifications to the nominal FCC-hh beam screen structure. The contribution of the pumping holes present in the outer chamber has been neglected since it has been shown to represent only a minor contribution to the resistive wall impedance [5]. The sawtooth pattern imprinted on the 75 μm Cu of the outer chamber has been simplified as a smooth surface since previous measurements [27] have shown that it does not significantly alter the surface impedance. The 75 μm thick Cu layer on the outer chamber has been reduced to an effective thickness of 50 μm, to take into consideration that during the manufacturing process there might be an effective mixture with stainless steel resulting in a heterogeneous layer [26, 28]. In addition, as suggested by [26] and [3], the exposed stainless steel at the open edges of the C-shaped inner chamber susceptible to increase the resistive wall beam impedance has been coated with 100 μm thick Cu.

Following the aforementioned considerations, we have calculated the resistive wall beam impedances using Eqs. (7) and (8) employing a simplified two-dimensional closed structure of the FCC-hh beam screen as illustrated in Fig. 2, for which we obtained $|H_{1s}|$. We have assumed a temperature of 50 K, where we consider that the thick wall approximation is valid for Cu at all frequency ranges of interest, except at the outer chamber where the Z_s function in Eqs. (7) and (8) is extended to a bilayer problem and evaluated using the generalized multilayer surface impedance theory [29]. For REBCO-CC, the London penetration depth λ_L, which is frequency independent, is lower than 200 nm; thus, it is smaller than the REBCO-CC thickness of about 2.5 μm.

## 3 Evaluation of surface impedance at FCC-hh conditions

The electromagnetic response of a surface with finite conductivity can be described by its surface impedance $Z_s = R_s + i X_s$, where R_s is the surface resistance and X_s is the surface reactance. As expressed in Eq. (7) and (8) surface impedance is one of the determining parameters for the calculation of the resistive wall beam impedance. Therefore, knowledge of REBCO-CC surface impedance is crucial when applied as coatings for the FCC-hh beam screen.

The surface impedance of REBCO-CC has to be determined under the extremely challenging operating conditions of the FCC-hh: at 50 K, under external magnetic fields of up to 16 T for frequencies extending from ≈ 2 kHz to ≈ 3 GHz, and azimuthal magnetic field strength between 130-230 A/m [30].

Several REBCO-CC, that differ in their architecture and superconducting properties have been studied [6, 30, 31] within the framework of the FCC-hh design studies. In those studies, it was shown that Fujikura tapes with artificial pinning centers (Fujikura APC) [32] are good representatives of REBCO-CC with one of the lowest surface impedance measured. Results in this paper have been obtained from data measured in Fujikura APC sample.

The proposal of utilizing REBCO-CC requires specialized technological advancements in the way of preparation. The REBCO-CC (shown in the top of Fig. 3) undergoes a delamination procedure to expose the REBCO (made of 2.5 μm thick EuBaCuO), directly to the beam (in the FCC-hh). Specific details of the procedure can be found in [33]. The result of the delamination procedure

Fig. 3 Top: Fujikura APC structure adapted from [32]. Bottom: end result of de-laminated Fujikura APC on a metal carrier. Schematic of de-laminated REBCO-CC on metal carriers
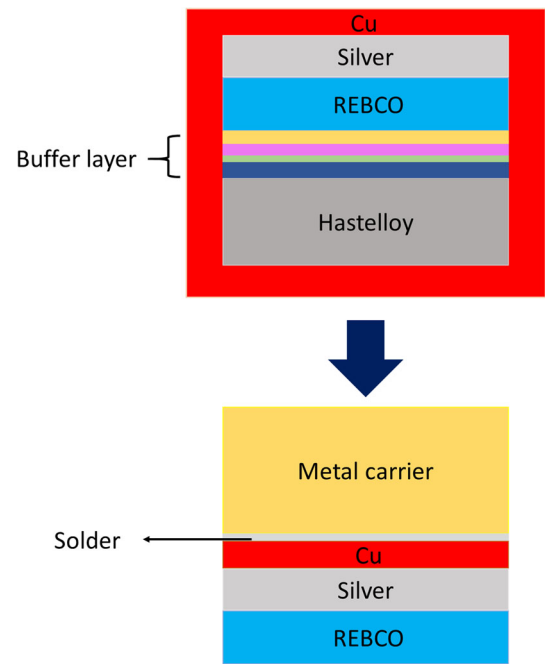
is schematically shown in the bottom of Fig. 3. In this figure, the REBCO-CC is attached to a metal carrier, such as the beam screen, using a solder specifically chosen to ensure adequate thermal contact and mechanical stability during a magnetic quench.

The surface resistance R_s of superconductors can be phenomenologically expressed as

$$R_s = R_{s,0} + R_{s,B},\tag{9}$$

where $R_{s,0}$ represents the surface resistance at 0 T which, according to the BCS model, may depend on the intrinsic properties of the superconductors. It may additionally contain residual surface resistance from external effects arising from weak links, defects, or twin boundaries of the material. $R_{s,B}$ denotes the field-dependent surface resistance mainly attributed to the creation and movement of quantized vortices or fluxons in the case of high-temperature superconductors.

The surface impedance data of de-laminated Fujikura APC used in this paper has been obtained in the frequency range from 6.5 to 13.6 GHz, at a temperature of 50 K, with magnetic fields up to 16 T, and very low VNA output power of -10 dBm to be in the linear regime [34]. The measurement was performed using a multimodal dielectric resonator [34] to achieve variable frequency measurement. Magnetic field dependence of the surface impedance was achieved using a ICEoxford High performance Cryogenic system$^{\circledR}$(HPCS).

At zero magnetic field, we have measured $R_{s,0} = 170(\pm 78)\,\mu\Omega$ at 8 GHz and 50 K. The frequency dependence of $R_{s,0}$ has been taken to follow a f^2 dependence commonly observed in REBCO theoretically and experimentally [35]. Moreover, we measured at different frequencies under an applied magnetic field and obtained the following relation: $R_{s,B} \propto f^{1.28(\pm 0.05)}B^{1.01(\pm 0.02)}$ with $R_{s,B} = 2.80(\pm 0.26)\,m\Omega$ at 16 T, 50 K, and 8 GHz. To our knowledge, these are the first results ever of surface resistance measured in high-temperature superconductors at 16 T in the GHz range.

Additionally, we measured the change of surface reactance with respect to the applied magnetic field through measurements at 8 GHz and 10 GHz and up to 9 T. Analogous to Eq. (9), the surface reactance X_s can be described as $X_s = \Delta X_{s,0} + X_s$, where $X_{s,0} = 2\pi f \mu_0 \lambda_L$. In this equation, μ_0 is the permeability of free space, and λ_L is the London penetration depth that can be written as $\lambda_L = \lambda_0/\sqrt{1-(T/T_c)^4}$, where $\lambda_0 = 150$ nm is the standard penetration depth at 0 K of REBCO and T_c is the critical temperature. We measured $\Delta X_s \propto f^{1.04(\pm 0.05)}B^{0.86(\pm 0.02)}$.

On the other hand, for Cu, we used measured R_s values of the FCC-hh Cu taken from [30]. For stainless steel, we used the resistivity of P506 SS grade obtained in [36]. Thus, we employed surface resistance values of Cu and stainless steel at 50 K of $R_s^{Cu} = 7.80(\pm 0.40)\,m\Omega$ and $R_s^{SS} = 137.6\,$mΩ, respectively. Additionally, we assumed $R_s = X_s \propto \sqrt{f}$ as for normal metals. The magneto-resistance of Cu has been shown to be negligible [30]. The magneto-resistance of SS stainless steel can also be neglected [36]. Therefore, we consider a magnetic field-independent surface impedance for these materials.

Using the measured data for Z_s, between 6 and 14 GHz, the results have been extrapolated to the range of interest, between 1 kHz and 100 GHz. In the extrapolation to low frequencies, we did not take into account extra effects that may arise at the foreseen operating temperature from flux creep phenomena, and which cannot be evaluated in our experiments. Furthermore, of specific interest for the FCC-hh are the values of the surface impedance at 1 T and at 16 T, which are the dipole magnetic fields at injection and collision energies. The extrapolated Z_s is shown in Fig. 4, where markers depict the measurements, solid lines present the

Fig. 4 Surface impedance used in the evaluation of resistive wall beam impedance obtained at 50 K. Markers depict measured R_s and X_s. Solid lines depict R_s. Dashed lines illustrate X_s. Black, red, green, purple, and light green colors represent stainless steel, copper, REBCO-CC at 16 T, REBCO-CC at 1 T, and REBCO-CC at 0 T, respectively. The inset zoomed the area close to the markers
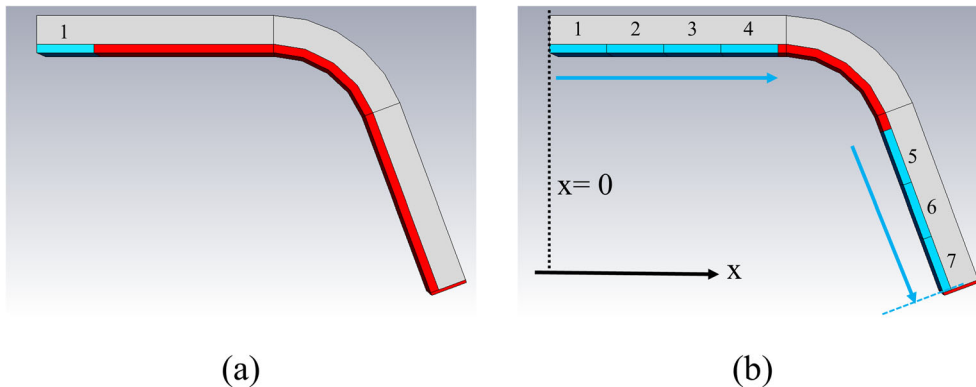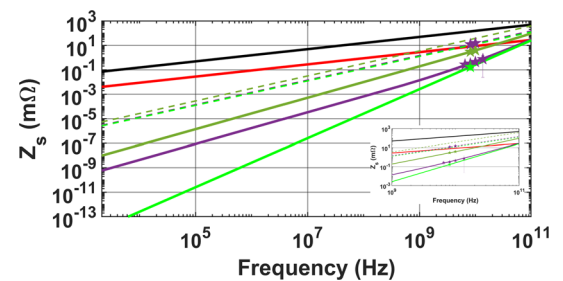

(a)   (b)

Fig. 5 Cross sectional view of the FCC-hh Cu with REBCO-CC in cyan and Cu in red. **a** Position 1. **b** All positions. The systematic position-dependent study is performed by varying the position of a 2-mm wide strip REBCO-CC from position 1 in (a) toward the edge of the inner chamber indicated by position 7 in (b), where (b) illustrates the positions being studied

surface resistance, and dashed lines describe the surface reactance. It is worth noting that the magnetic field in the measurements is always applied perpendicular to the surface of the REBCO-CC samples, which is the orientation that gives the highest surface impedance [37]. This implies that we have used a rather conservative value of surface impedance in our calculations.

4 Impact of REBCO-CC position, content, and manufacturability on the resistive wall beam impedance

In this section, we present a systematic study of the effect on the resistive wall beam impedance when placing REBCO-CC at various BS sections and also with varying REBCO-CC content. In these calculations, we have used a beam screen configuration with 100-μm thick Cu open edges and have neglected the potential effects of an aC coating in this simplified model. Moreover, we investigate the effect of open edges with exposed stainless steel and the effect of manufacturability by investigating the solder residues after fabrication. It is important to note that in this section, we used the surface impedance of REBCO-CC at 0 T. While we only show the inner chamber in the figures, the calculations were performed over the entire sections of the BS that is, including the outer chamber as shown in Fig. 2.

4.1 Effect of REBCO-CC position

We examine the impact of the position of REBCO-CC on the resistive wall beam impedance while keeping REBCO-CC content constant, by employing a 2-mm wide strip of REBCO-CC on the inner chamber of the beam screen. This 2-mm strip is placed symmetrically; and therefore, we only illustrate it for one quadrant of the FCC-hh beam screen see Fig. 5. The rest of the inner chamber is made of Cu.

Firstly, we define positions from 1 to 7, with position 1 starting at the top center of the inner chamber as depicted in Fig. 5a. The 2-mm strip is then positioned following the direction of the arrow until the last position, position 7, as shown in Fig. 5b. Positions 1 to 4 are located at the top section of the inner chamber; whereas, positions 5 to 7 are situated at the diagonal section of the inner chamber. The curved sections of the inner chamber are not foreseen to be coated with REBCO-CC, since curving the REBCO-CC potentially alters their microwave properties.

To demonstrate the impact of the REBCO-CC position, the relative percentage difference is calculated at each position compared to a full Cu beam screen. The calculation is performed through $Z_{i,RelDiff} = \frac{Z_{i,position} - Z_{i,Cu}}{Z_{i,Cu}}$, where $i = x$, y, z at a representative

Fig. 6 Relative percentage difference of resistive wall beam impedances of the FCC-hh beam screen calculated at 1 GHz
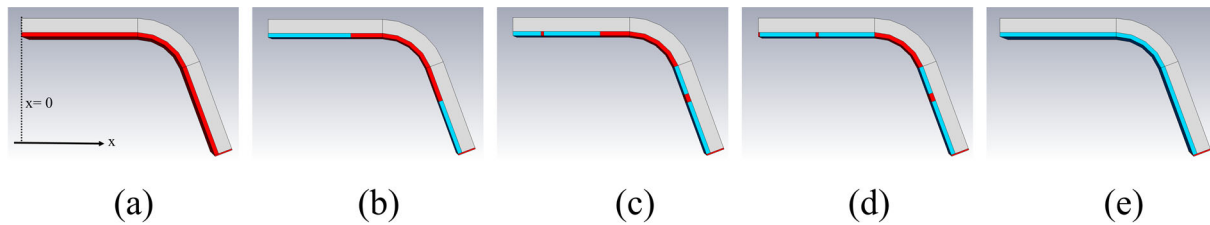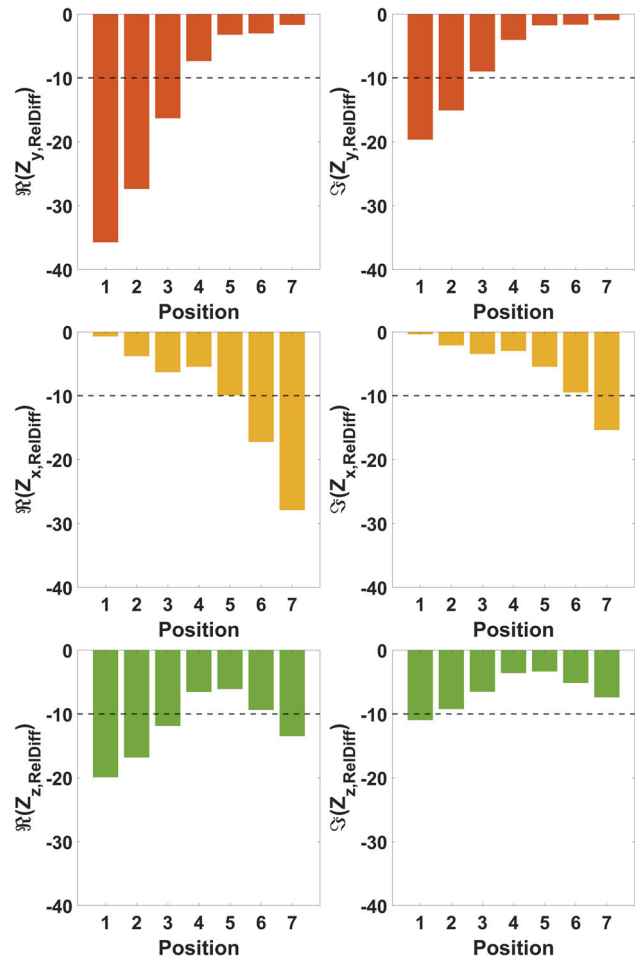

Fig. 7 Models of various configurations taken from CST with **a** 0% REBCO-CC (Full Cu), **b** 53% REBCO-CC, **c** 63% REBCO-CC, **d** 73% REBCO-CC, and **e** 100% REBCO-CC (Full REBCO-CC). Red colored surfaces depict Cu. Cyan colored surfaces illustrate REBCO-CC

frequency which is at 1 GHz. With a 2-mm strip, we find that a 10% reduction (indicated by the black horizontal dashed line) is large enough to describe which are the significant positions.

Figure 6 presents the $Z_{i,RelDiff}$ in all planes for the different positions of the 2-mm strip. In general, reductions can be observed in all planes. Multiple positions demonstrate a reduction above 10% in the real part, owing to its lower surface resistance, compared to the imaginary part. Maximum reductions can be observed in both Z_y and Z_z when the 2-mm strip is positioned at position 1. Whereas, a maximum reduction can be seen in Z_x at position 7. Reductions above 10% in the real part of Z_y can be observed at positions 1-3, while positions 6-7 for Z_x. As for the real part of Z_z, reductions above 10% can be seen in positions 1–3 and 7.

In summary, the positions relevant for reductions of Z_y, Z_x, and Z_z are positions 1–3 and 6–7. These are the positions at the top section of the inner chamber closest to the center (*i.e.*, $x = 0$), and the diagonal section closest to the open edge of Fig. 2.

4.2 Effect of REBCO-CC content

Following the position-dependent studies performed in Sect. 4.1, we define several configurations. Firstly, 0% REBCO-CC content (full Cu) and 100% REBCO-CC content (full REBCO-CC) beam screen are included, which provides the upper and lower bound of the resistive wall beam impedance. The next configuration consists of 53% of REBCO-CC with REBCO-CC placed at significant

Fig. 8 Resistive wall beam impedances for various REBCO-CC content described in Fig. 7. Solid lines present the real part. Dashed lines depict the imaginary part
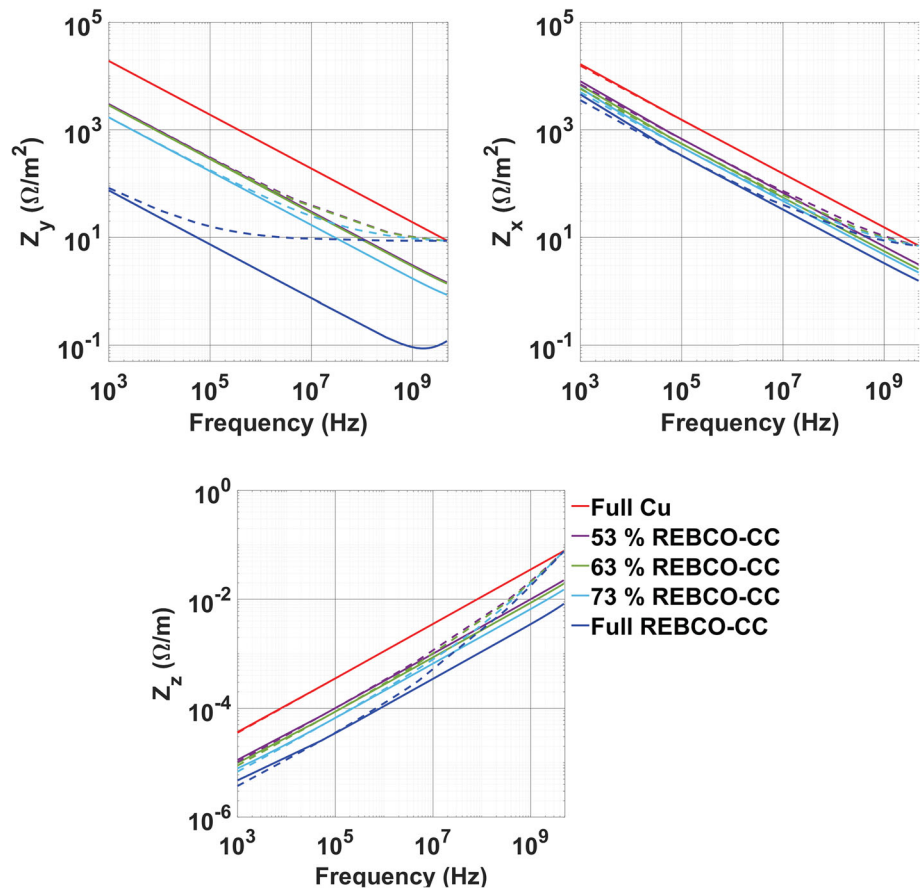

positions emphasized in Sect. 4.1. It has a 6-mm wide REBCO-CC strip at the top section of the inner chamber and a 4-mm wide REBCO-CC strip at the diagonal section. We then increased the REBCO-CC content to 63 and 73% REBCO-CC. The five configurations are illustrated in Figs. 7a–e. We note that subdividing the REBCO-CC into narrow strips has been shown to overcome shortcomings on the magnetic field quality that will be seen by the beam [7, 8]. Hence, 63% and 73% REBCO-CC configurations in Figs. 7c, d use 2- and 4-mm wide REBCO-CC. In order to fully decouple the REBCO-CC strips, a 200-μm wide Cu gap at the top section of the inner chamber and 600-μm wide Cu gap at the diagonal section are introduced in configuration (c). In configuration (d), two 200-μm wide Cu at the top section of the inner chamber and a 600-μm wide Cu gap at the diagonal section are introduced in 73% REBCO-CC between the REBCO-CC strips. One of the 200-μm wide Cu has its center aligned at $x = 0$. 200- and 600-μm wide Cu gap have been taken as possible typical values of the gap left after assembling the hybrid beam screen.

Figure 8 depicts the calculated resistive wall beam impedance Z_y, Z_x, and Z_z for the different beam screen configurations considered. It can be seen that the resistive wall beam impedance, both the real and the imaginary parts, decreases gradually in all three planes with increasing REBCO-CC content. A notable reduction is observed in Z_y, followed by Z_z, and then Z_x. It can be noticed in Fig. 8 that contrary to the full Cu beam screen where the difference between Z_y and Z_x is small, the hybrid beam screens (53% - 73% REBCO-CC) present large differences between the two transversal planes. As the REBCO-CC content increases, this difference is further enhanced. It turns out that this outcome is attributed mainly to the contribution of Cu at the outer chamber evident from the results of the full REBCO-CC coated beam screen in Fig. 8. Even with this full REBCO-CC coating in the inner chamber, the real part of Z_x can only be reduced at most by a factor of 5 at 5×10^5 Hz. The contribution of Cu in the outer chamber also limits Z_z, wherein one can find a factor of 10 reductions for the full REBCO-CC beam screen also at 5×10^5 Hz.

Although there are large differences in the magnitude of Z_y and Z_x for the studied hybrid beam screens, in general, for the real part, their frequency dependence behaves the same; all lines being parallel to the full Cu beam screen resistive wall beam impedance. This trend is also evident in the full REBCO-CC beam screen at low frequencies, except above 1 GHz where one can notice an increase in slope. This shift is understood to be due to the frequency dependence of REBCO-CC surface impedance. As for the imaginary part, Z_y and Z_x tend to converge toward the frequency dependence of the full Cu beam screen at low frequencies; whereas, they converge toward the full REBCO-CC beam screen at high frequencies. This can also be observed in Z_z. These findings are consistent with studies performed in the hybrid elliptical beam screen [12], wherein there is a crossover from a regime dominated by the frequency behavior of Cu at lower frequencies to a regime dominated by the behavior of the REBCO-CC at high frequencies.

Fig. 9 Effect of exposed stainless steel on the horizontal resistive wall beam impedance. **a** 73% REBCO-CC BS with exposed stainless steel in gray. **b** Effect of exposed SS through comparison of Cu configuration coated with Cu at the open edges in red, 73% REBCO-CC with exposed SS in purple, and 73% REBCO-CC with Cu-coated open edges in cyan. Solid lines present the real part. Dashed lines depict the imaginary part
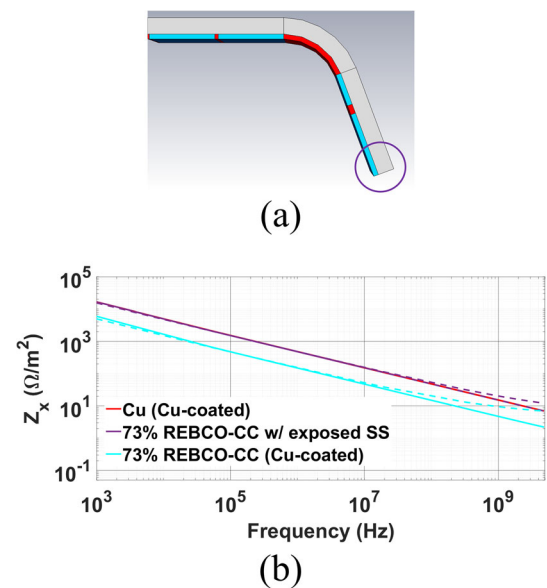
From the point of view of reducing the resistive wall beam impedance, a 100% REBCO-CC coating would be desirable. However, it has been shown [38] that this coating will not fulfill the specifications on the magnetic field quality. The highest REBCO-CC content that meets the magnetic field quality and lowers the resistive wall impedance the most is the 73% REBCO-CC beam screen, presented in Fig. 7d. We expand the study of this configuration by investigating potential risks due to fabrication and exposed stainless steel, and evaluating its impact on the FCC-hh operation conditions.

4.3 Effect of open edges with exposed stainless steel

Although exposed stainless steel (SS) has previously [26] been shown to increase the resistive wall beam impedance horizontally in a full Cu beam screen, we studied its effect on the resistive wall beam impedance of a hybrid beam screen. We have taken a 73% REBCO-CC beam screen and used stainless steel on the open edges, as shown in Fig. 9a. Figure 9b displays the horizontal resistive wall beam impedance as it is the beam impedance most affected by this change. It can be observed that the impedance of the 73% REBCO-CC beam screen with exposed stainless steel is higher, by a factor 3, compared to the 73% REBCO-CC beam screen coated with Cu at the open edges. This increase is significant, resulting in a value comparable to the one of a full Cu beam screen. The longitudinal resistive wall beam impedance, is also affected, increasing by a factor of 3, while the vertical resistive wall impedance only increases by a factor 1.1. These results imply that exposed stainless steel degrades the beam impedance to the point where the use of REBCO-CC is meaningless to reduce the horizontal resistive wall beam impedance.

We strongly recommend that any further development of the beam screen, considers coating any open edges with highly conducting material, such as Cu or REBCO-CC.

4.4 Effect of manufacturability

The hybrid beam screen configuration shown in Fig. 7d with Cu open edges has been used to study the potential effect of solder residues after fabricating the hybrid beam screen. We assume that a 100-μm wide gap of solder may leak on each side of the REBCO-CC. For simplicity, we demonstrate the effect of solder residues by increasing the surface resistance of these 100-μm wide gaps to thrice [38] the surface resistance of Cu and subsequently compute the relative difference in percentage of the resistive wall beam impedance due to this change. We want to emphasize at this point that the effect of soldering residues on the manufacturability have only been considered in relation to the changes introduced in the resistive wall impedance. We acknowledge that the presence of such residues would also have an important contribution to the geometrical impedance [39] which has not been considered here as our conclusions are primarily based on resistive wall impedance.

Figure 10 shows the vertical resistive wall beam impedance of 73% REBCO-CC beam screen with solder residues compared to Cu and 73% REBCO-CC beam screen without solder residues. It can be observed that the presence of solder increases the vertical resistive wall beam. The maximum increase in the real part, approximately by 105% is found at 6×10^8 Hz and an increase of 101% is found at 2.1×10^3 Hz for the imaginary part. The horizontal and longitudinal resistive wall beam impedances, on the other hand, increase less than 50%. Nonetheless, all resistive wall impedances remain lower than that of a full Cu beam screen.

Fig. 10 Effect of solder residues through comparison of Cu configuration in red, 73% REBCO-CC with solder residues in black, and 73% REBCO-CC without solder residues in cyan. Dashed lines depict the imaginary part. All the configurations have Cu-coated open edges. Solid lines present the real part
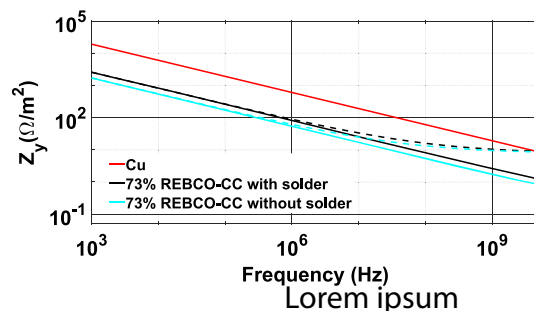

Table 1 Summary of the ratio of growth rates between a full Cu beam screen and a 73% REBCO-CC beam screen at coupled-bunch frequency for injection and collision energies

Plane	Ratio	Injection, 1 T	Collision, 16 T
x	$\dfrac{\tau_{y,Cu}^{-1}}{\tau_{y,73\%REBCO-CC}^{-1}}$	11.2	11.2
y	$\dfrac{\tau_{x,Cu}^{-1}}{\tau_{x,73\%REBCO-CC}^{-1}}$	2.8	2.8

5 Impact of the resistive wall beam impedance at the operating conditions of the FCC-hh

We have calculated the resistive wall beam impedance for a beam screen with 73% of REBCO-CC in the inner chamber and any exposed open edge is coated with Cu, at injection and collision energies, which correspond to dipolar magnetic fields of 1 T and 16 T, respectively. We adopt here the correspondence between the beam energy (injection and collision) and the magnetic field (1 T and 16 T) since this is the parameter that changes the surface impedance at these operating conditions.

The vertical resistive wall beam impedance, Z_y, identified as the most critical one for the FCC-hh [5], contributing significantly to the transverse coupled-bunch impedance budget at both injection and collision energies, while the transverse mode coupling instability, that can cause a single bunch effect, contributes mainly at injection limiting the maximum bunch current attainable.

The most unstable mode of the couple bunch instability at zero chromaticity, can be proven to be roughly proportional [36] to the real part of the beam coupling impedance evaluated at the lowest betatron sideband $f_c = (1 - Q)f_0$ where f_0 is the revolution frequency and Q is the fractional part of the betatron tune, which results in $f_c = 2.1$ kHz. In the following, we compare the growth rate of the coupled-bunch instability of a 73% REBCO-CC beam screen with a 100% Cu beam screen using,

$$\frac{\tau_{y,Cu}^{-1}}{\tau_{y,73\%REBCO-CC}^{-1}} = \frac{\Re(Z_{y,Cu})}{\Re(Z_{y,73\%REBCO-CC})}. \tag{10}$$

We note that Eq. (10) is an oversimplification, and it only reflects the ratio between two beam screen configurations with different surface impedance while neglecting all other parameters that might also contribute to the impedance growth rate. Nonetheless, since the beam screen's resistive wall beam impedance is the main contributor to the beam impedance budget [5], we believe that the expression in Eq. (10) might allow an adequate comparison between a hybrid and a pure Cu beam screen.

Table 1 summarizes the ratio of coupled-bunch instabilities growth rates between a full Cu and a 73% REBCO-CC beam screens at injection and collision energies.

The analysis reveals that the growth rate ratio of the coupled-bunch instability is independent of the magnetic field, and thus, of the beam energy. In the vertical plane we observe one order of magnitude reduction in the growth rate compared to that of the full Cu beam screen. In the horizontal plane, a three-fold reduction in the growth rate is observed. The Cu contribution from the outer chamber limits the resistive wall beam impedance of a hybrid beam screen and therefore even if the surface impedance of REBCO-CC is orders of magnitude lower compared to Cu (Fig. 4) at low frequencies, the beam impedance does not decrease accordingly. Nonetheless, these results show a reduction in the growth rate compared to Cu independent of the magnetic field. This would mean that there could be a potential margin for an increase in the dipole magnetic field, hence, the collision energy (*e.g.,* as the FCC-hh 20 T magnetic field scenario [40]).

On the other hand, the single bunch instability, and therefore the maximum achievable bunch current, is governed by the imaginary part of the transverse resistive wall beam impedance. To achieve optimal bunch intensity threshold, it is desirable to minimize the imaginary part of the impedance as possible. Although the FCC-hh beam screen's effect on the bunch intensity threshold is small compared to other accelerator components, it is still considerable [5, 36]. In Fig. 11, we compare the imaginary parts of Z_y and Z_x between full Cu and 73% REBCO-CC beam screens at injection and collision energies. It is evident that the imaginary parts of 73% REBCO-CC beam screen remain lower compared to Cu across nearly all frequencies of interest. These findings suggest that REBCO-CC coating enhances the bunch intensity threshold, potentially increasing the collision rate in the FCC-hh.

Fig. 11 Resistive wall beam impedances at injection (1 T) and collision (16 T) energies for a 73% REBCO-CC beam screen compared to 100% Cu beam screen. Solid lines present the real part. Dashed lines depict the imaginary part. The orange vertical dashed line highlights the coupled-bunch frequency
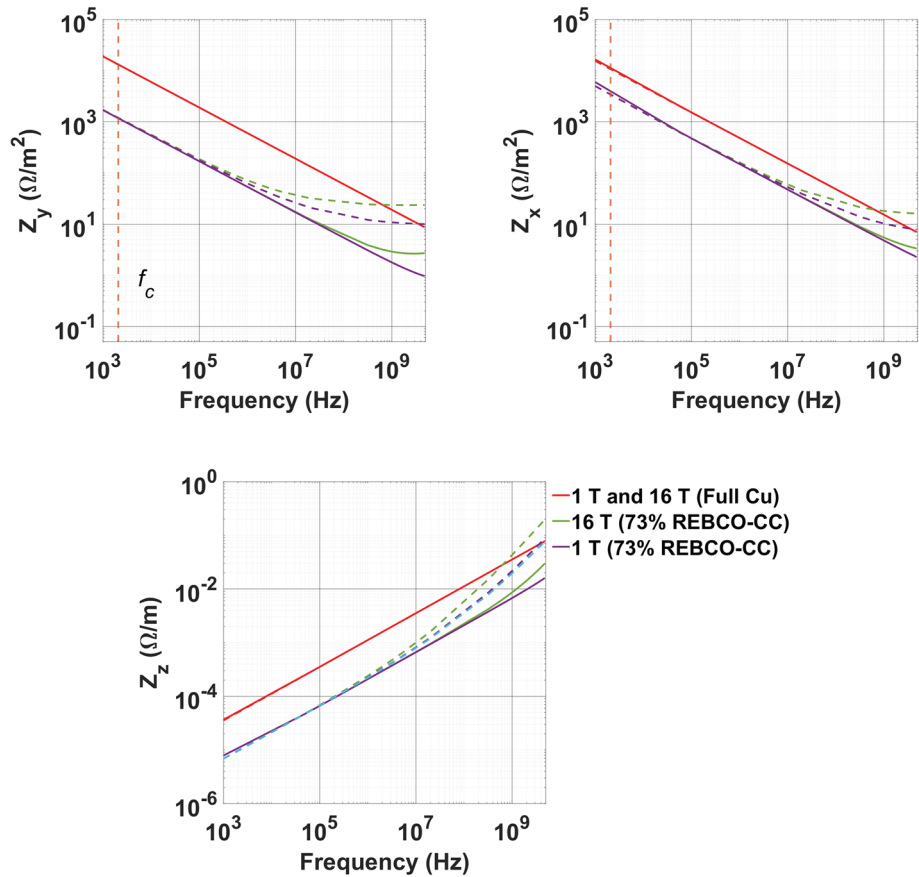
Table 2 Energy loss ratio between full Cu- and 73% REBCO-CC beam screen

Energy	$\frac{\Delta E_{Cu}}{\Delta E_{73\%REBCO-CC}}$
Injection energy	5.3
Collision energy	5.1

The real part of the longitudinal resistive wall beam impedance, $\Re(Z_z)$, can be used to determine the energy loss in the FCC-hh due to the image current. The energy loss for a Gaussian bunch per revolution turn can be described by,

$$\Delta E \propto \int_0^\infty \Re(Z_z(f))e^{-4\pi^2 f^2 \sigma_\tau^2} df \tag{11}$$

where the value of the bunch length (σ_τ) is 1.07 ns for the FCC-hh and f is the frequency. The ratio of the energy loss between a 73% REBCO-CC beam screen and a 100% Cu beam screen can be computed as the ratio of the real part of the longitudinal beam impedance as given in Fig. 11. Since $\Re(Z_z)$ is independent of the magnetic field below 100 MHz, and only shows a small dependency above 1 GHz, the ratio of energy loss at injection and collision energies is almost the same, as shown in Table 2. The heat load due to the image currents reduces by a factor of five when using a 73% REBCO-CC beam screen compared to a full Cu beam screen.

For completeness, we include the effect of coating the beam screen with a thin layer of amorphous carbon. To calculate the impact of such an aC layer on the resistive wall beam impedance, we coat the top and bottom sections of the inner chamber, including its curved corners, with Ti-aC layers. These are the sections of the inner chamber critical for electron cloud build-up and have been suggested to be coated by [3]. In our calculations, we use aC thickness of 100 nm and Ti thickness of 150 nm, although thinner coatings can also be produced [6]. The surface impedances of aC and Ti are derived from the knowledge of their skin depths, which are experimentally estimated in [6] at 50 K and 8 GHz to be about 23 μm and 1 μm, respectively.

Figure 12 shows the resistive wall beam impedances in the three planes for the beam screens with and without Ti-aC coating comparing the results of a fully coated Cu BS with a 73% REBCO-CC content BS. On the real part, it can be observed that Ti-aC beam screens do not significantly alter the resistive wall beam impedance in the three planes. On the imaginary part, it can be observed that below 10^7 Hz, there are no changes in the resistive wall beam impedance. However, above 10^7 Hz, the difference between with and without Ti-aC coating increases with increasing frequency. The largest difference can be observed in the imaginary part of Z_y at injection energy amounting to a factor of 2.2 at 3 GHz. We emphasize that the baseline design made of Cu also requires

Fig. 12 Resistive wall beam impedances at injection (1 T) in purple and collision (16 T) energies in green for a 73% REBCO-CC beam screen compared to a full Cu beam screen in red. Solid lines show those without Ti-aC coating. Dashed lines depict those with Ti-aC coating
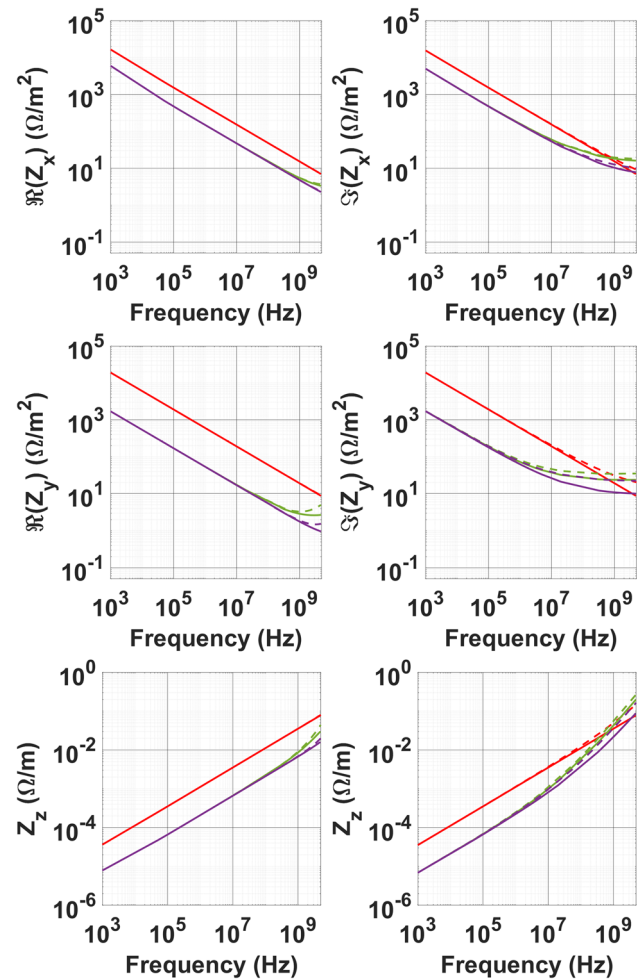
the aC coating, which increases its resistive wall beam impedance by a factor of 2; and therefore, REBCO-CC beam screen remains lower than Cu beam screen.

6 Conclusion

We have investigated the impact of hybrid REBCO-CC-Cu on the resistive wall beam impedance of the FCC-hh nominal beam screen design, employing values of REBCO-CC obtained at experimental conditions as close as possible to the working conditions of the FCC-hh. We have combined CST and the generalized beam coupling impedance theory to calculate the resistive wall beam impedance of the complex FCC-hh beam screen structure.

We have optimized the hybrid REBCO-CC-Cu content distribution by performing a position and REBCO-CC content study, identifying the significant positions where REBCO-CC significantly reduces the resistive wall beam impedances. In addition, by studying a full REBCO-CC inner chamber, we found that the resistive wall beam impedance is still limited by the contribution of Cu from the outer chamber. The analysis of results demonstrated that a 73% REBCO-CC content is the maximum one that reduces resistive wall beam impedance the most and, at the same time, satisfies the magnetic field quality criteria. By employing this content, the resistive wall beam impedance presents reduced growth rates, increased bunched intensity, and low heat load compared to that of a full Cu beam screen. It has also been observed that the resistive wall beam impedance for all three planes is nearly independent of the magnitude of the dipole magnetic field, which may suggest there is still potential room for an increase in the collision energy. This remains true even when the beam screen is coated with titanium and amorphous carbon layers.

Besides the limitation in the resistive wall beam impedance due to the presence of Cu in the outer chamber, we have investigated the impact of the surface resistance of exposed stainless steel and of the possible solder residues after fabrication. In the case of the exposed stainless steel open edges, the simulations show a significant increase in resistive wall beam impedance to the point that it renders the coating with REBCO-CC meaningless, at least in the horizontal plane. These open edges will have to be covered with highly conducting materials to ensure beam stability. On the other hand, when the solder residues are present, large increase in

the vertical resistive wall beam impedance can be observed to about 105% in both real and imaginary parts. These results suggest avoiding solder residue as much as possible.

Our conclusions are based on resistive wall impedance and on the potential beneficial impact of using REBCO-C as beam screen, which has not yet been implemented in any accelerator. We acknowledge that other forms of impedance could influence the results presented here and further studies will be required in the future.

We have demonstrated in this study that by using REBCO-CC, the resistive wall beam impedance in a 73% REBCO-CC beam screen outperforms the behavior of the Cu beam screen.

Data availability This manuscript has no associated data or the data will not be deposited. The authors declare that all the relevant data are either reported in the paper or can be derived employing a numerical approach described using the theory referred to and the software cited.

Material availability Not applicable.

Declarations

Conflict of interest The authors have no relevant financial or non-financial interests to disclose.

Ethical approval and consent to participate Not applicable.

Consent for publication Not applicable.

References

1. A. Abada et al., FCC-hh: the Hadron collider: future circular collider conceptual design report volume 3. Euro. Phys. J. Special Topics **228**(4), 755–1107 (2019)
2. P. Gan, K. Zhu, Q. Fu, H. Li, Y. Lu, M. Easton, Y. Liu, J. Tang, Q. Xu, Design study of an YBCO-coated beam screen for the super proton-proton collider bending magnets. Rev. Sci. Instrum. **89**(4), 045114 (2018). https://doi.org/10.1063/1.5026932
3. I. Bellafont, M. Morrone, L. Mether, J. Fernández, R. Kersevan, C. Garion, V. Baglin, P. Chiggiato, F. Pérez, Design of the future circular hadron collider beam vacuum chamber. Phys. Rev. Accel. Beams **23**(3), 033201 (2020)
4. C. Yin Vallgren, G. Rumolo, K. Cornelis, P. Costa Pinto, J. Bauche, P. Chiggiato, M. Taborelli, G. Arduini, S. Calatroni, H. Neupert et al., Amorphous carbon coatings for the mitigation of electron cloud in the CERN super proton synchrotron. Phys. Rev. Spec. Top. Accel. Beams **14**(CERN–OPEN–2011–040), 071001 (2011)
5. S. Arsenyev, D. Schulte, O. Boine-Frankenheim, FCC-hh transverse impedance budget. In: 9th International particle accelerator conference (IPAC'18), Vancouver, BC, Canada, 2018, pp. 149–152 (2018). JACOW Publishing, Geneva, Switzerland
6. T. Puig, P. Krkotić, A. Romanov, J. O'Callaghan, D. Zanin, H. Neupert, P. Pinto, P. Demolon, A.G. Costa, M. Taborelli et al., Coated conductor technology for the beamscreen chamber of future high energy circular colliders. Supercond. Sci. Technol. **32**(9), 094006 (2019)
7. G.T. Telles, A. Romanov, S. Calatroni, X. Granados, T. Puig, J. Gutierrez, Field quality and surface resistance studies of a superconducting $REBa_2Cu_3O$-Cu hybrid coating for the FCC beam screen. Supercond. Sci. Technol. **36**(4), 045001 (2023)
8. S. Patsch, U. Niedermayer, W.D. Stem, O. Boine-Frankenheim, Computation of the magnetization of type II superconductors for potential beam screen coatings of the future circular collider. IEEE Trans. Appl. Supercond. **29**(6), 1–10 (2019)
9. M. Haubner, P. Krkotić, C. Serafim, V. Petit, V. Baglin, S. Calatroni, B. Henrist, A. Romanov, T. Puig, J. Gutierrez, Electron beam characterization of rebco-coated conductors at cryogenic conditions. Appl. Sci. **13**(5), 2765 (2023)
10. P. Krkotić, U. Niedermayer, O. Boine-Frankenheim, High-temperature superconductor coating for coupling impedance reduction in the fcc-hh beam screen. Nucl. Instrum. Methods Phys. Res., Sect. A **895**, 56–61 (2018)
11. P. Krkotić, N.D. Tagdulang, S. Calatroni, J.M. O'Callaghan, M. Pont, Potential impedance reduction by REBCO-coated conductors as beam screen coating for the future circular hadron collider. Europhys. Lett. **140**(6), 64001 (2022). https://doi.org/10.1209/0295-5075/acaac3
12. N. Tagdulang, T. Günzel, P. Krkotić, J.M. O'Callaghan, Pont, M.: Evaluation of the impact of REBCO-coated conductors on the resistive wall impedance of the FCC-hh. J. Phys.: Conf. Ser. 2687(6), 062014 (2024). https://doi.org/10.1088/1742-6596/2687/6/062014
13. R.L. Gluckstern, J. Zeijts, B. Zotter, Coupling impedance of beam pipes of general cross section. Phys. Rev. E **47**(1), 656–663 (1993). https://doi.org/10.1103/PhysRevE.47.656

14. T.B.A. Senior, J.L. Volakis, *Approximate Boundary Conditions in Electromagnetics* (United Kingdom, IET, 1995), p.14

15. K. Fujita, Impedance computation of cryogenic vacuum chambers using boundary element method. Phys. Rev. Accel. Beams **25**(6), 064601 (2022). https://doi.org/10.1103/PhysRevAccelBeams.25.064601

16. R.L. Gluckstern, Analytic methods for calculating coupling impedances (2000). https://doi.org/10.5170/CERN-2000-011

17. M. Migliorati, L. Palumbo, C. Zannini, N. Biancacci, V.G. Vaccaro, Resistive wall impedance in elliptical multilayer vacuum chambers. Phys. Rev. Accel. Beams **22**(12), 121001 (2019). https://doi.org/10.1103/PhysRevAccelBeams.22.121001

18. CST - Computer Simulation Technology, Dassault Systems, 2020. https://www.cst.com/

19. C. Zannini, Electromagnetic simulation of CERN accelerator components and experimental applications. Ph.D. Thesis, Ecole Polytechnique, Lausanne (2013). https://cds.cern.ch/record/1561199

20. U. Niedermayer, O. Boine-Frankenheim, H. De Gersem, Space charge and resistive wall impedance computation in the frequency domain using the finite element method. Phys. Rev. Spec. Top. Accel Beams **18**(3), 032001 (2015). https://doi.org/10.1103/PhysRevSTAB.18.032001

21. R. Wanzenber, A. Rajabi, Resistive wall impedance of multilayer beam pipes of general cross sections, 3402–3404084. https://doi.org/10.18429/JACOW-IPAC2023-WEPL124

22. G. Iadarola, E. de la Fuente, L. Giacomel, C. Zannini, A generalized tool to compute wake potential and impedance from electromagnetic time domain simulations, 3522–352512. https://doi.org/10.18429/JACOW-IPAC2023-WEPL170

23. U. Niedermayer, Determination of beam coupling impedance in the frequency domain. Ph.D. Thesis, Technische Universität Darmstadt, Darmstadt (2016)

24. Doliwa, B., De Gersem, H., Weiland, T.: Numerical calculation of coupling impedances for kicker modules. In: Proceedings of the 2005 particle accelerator conference, pp. 1820–1822. IEEE, Knoxville, TN, USA (2005). https://doi.org/10.1109/PAC.2005.1590924

25. MATLAB - El lenguaje del cálculo técnico. https://es.mathworks.com/products/matlab.html

26. D. Astapovych, Collective effects in the hadron future circular collider. Ph.D. Thesis, Technische Universität Darmstadt, Darmstadt (2020). https://doi.org/10.25534/tuprints-00011786

27. F. Caspers, M. Morvillo, F. Ruggiero, J. Tan, H. Tsutsui, Surface resistance measurements of LHC dipole beam screen samples (2000)

28. N. Mounet, The LHC transverse coupled-bunch instability. Ph.D. Thesis, Ecole Polytechnique, Lausanne (2012). https://doi.org/10.5075/epfl-thesis-5305

29. P. Krkotic, Evaluation of the surface impedance of ReBCO coated conductors and requirements for their use as beam screen materials for the FCC-hh. Ph.D. Thesis, Universitat Politècnica de Catalunya (2022). https://doi.org/10.5821/dissertation-2117-380818

30. P. Krkotić, A. Romanov, N. Tagdulang, G. Telles, T. Puig, J. Gutierrez, X. Granados, S. Calatroni, F. Perez, M. Pont, J.M. O'Callaghan, Evaluation of the nonlinear surface resistance of REBCO coated conductors for their use in the FCC-hh beam screen. Supercond. Sci. Technol. **35**(2), 025015 (2022). https://doi.org/10.1088/1361-6668/ac4465

31. A. Romanov, P. Krkotić, G. Telles, J. O'Callaghan, M. Pont, F. Perez, X. Granados, S. Calatroni, T. Puig, J. Gutierrez, High frequency response of thick REBCO coated conductors in the framework of the FCC study. Sci. Rep. **10**(1), 1–12 (2020)

32. Fujikura Ltd. https://www.fujikura.co.jp/

33. N. Llamas, Private communication

34. N. Tagdulang, Surface imepdance characterization of high-temperature superconducting coated conductors for potential application in the future circular collider beam screen. Ph.D. Thesis, Universitat Politècnica de Catalunya (2024)

35. M. Hein, *High-Temperature-Superconductor Thin Films at Microwave Frequencies*, vol. 155 (Springer, Berlin Heidelberg, 1999), p.723. https://doi.org/10.1007/BFb0111182

36. D. Astapovych, O. Boine-Frankenheim, V. Gubaidulin, V. Kornilov, U. Niedermayer, D. Schulte, Stability limits with Landau damping in the FCC-hh. J. Instrum. **16**(01), 01013 (2021)

37. Y. Noguchi, N. Sekiya, A. Saito, H. Yamasaki, Y. Nakagawa, S. Hirano, S. Ohshima, Dependence of the surface resistance and critical current density in HTS thin films on an angle of applied magnetic field. Physica C (Amsterdam, Neth.) **445–448**, 858–861 (2006). https://doi.org/10.1016/j.physc.2006.05.042

38. G. Telles, Ph.D. Thesis to be published. https://www.fujikura.co.jp/

39. A. Blednykh, G. Bassi, V. Smaluk, R. Lindberg, Impedance modeling and its application to the analysis of the collective effects. Phys. Rev. Accel. Beams **24**(10), 104801 (2021)

40. J. Nugteren, G. Kirby, J. Murtomäki, G. DeRijk, L. Rossi, A. Stenvall, Toward REBCO 20 T+ dipoles for accelerators. IEEE Trans. Appl. Supercond. **28**(4), 1–9 (2018)